NMR Solution Structure of Calcium-Saturated Skeletal Muscle Troponin C‡

Carolyn M. Slupsky and Brian D. Sykes*

MRC Group in Protein Structure and Function, Department of Biochemistry, University of Alberta, Edmonton, Alberta, Canada T6G 2H7

Received July 12, 1995; Revised Manuscript Received September 20, 1995®

ABSTRACT: Troponin C (TnC) is an 18 kDa (162-residue) thin-filament calcium-binding protein responsible for triggering muscle contraction upon the release of calcium from the sarcoplasmic reticulum. The structure of TnC with two calcium ions bound has previously been solved by X-ray methods. Shown here is the solution structure of TnC which has been solved using 3D and 4D heteronuclear nuclear magnetic resonance (NMR) spectroscopic techniques. The ^{1}H, ^{13}C, and ^{15}N backbone chemical shifts have already been published [Slupsky, C. M., Reinach, F. C., Smillie, L. B., & Sykes, B. D. (1995) *Protein Sci. 4*, 1279−1290]. Presented herein are the ^{1}H, ^{13}C, and ^{15}N side-chain chemical shifts which are 80% complete. The structure of calcium-saturated TnC was determined on the basis of 2106 NOE-derived distance restraints, 121 ϕ dihedral angle restraints, and 76 ψ dihedral angle restraints. The appearance of calcium-saturated TnC reveals a dumbbell-shaped molecule with two globular domains connected by a linker. The structures of the N-terminal and C-terminal domains are highly converged [backbone atomic root mean square deviations (rmsd) about the mean atomic coordinate position for residues 10−80 and 98−155 are 0.66 ± 0.17 and 0.69 ± 0.18 Å, respectively]; however, the orientation of one domain with respect to the other is not well-defined, and thus each domain appears to be structurally independent. Comparison of the calcium-saturated form of TnC determined herein with the half-saturated form determined by X-ray methods reveals two major differences. First, there is a major structural change which occurs in the N-terminal domain resulting in the opening of a hydrophobic pocket presumably to present itself to its target protein troponin I. This structural change appears to involve only helices B and C which move away from helices N/A/D by the alteration of the backbone ϕ, ψ angles of glutamic acid 41 from irregular in the crystal structure (−97°, −7°) to helical in the NMR calcium-saturated structure (−60°, −34°). The other difference between the two structures is the presence of a flexible linker between the two domains in the NMR structure. This flexible linker allows the two domains of TnC to adopt any orientation with respect to one another such that they can interact with a variety of targets.

Troponin C (TnC),[1] an 18 kDa protein, is the calcium-sensitive molecular trigger for muscle contraction. TnC contains two spatially independent calcium binding domains and is present in both fast twitch (skeletal) and cardiac muscles. TnC is a member of a trimer of proteins called the troponin complex (TnI and TnT being the other two components) which is anchored onto the actin filament and tropomyosin via the TnT subunit. Release of calcium by the sarcoplasmic reticulum results in the binding of calcium to TnC and the release of the inhibition of the actin−myosin interaction.

The crystal structure of skeletal TnC with its structural (C-terminal) calcium binding sites filled and the regulatory (N-terminal) calcium binding sites apo ($2Ca^{2+}$-TnC) has been solved (Herzberg & James, 1988; Satyshur et al., 1988, 1994). The C-terminal domain contains the high-affinity calcium/magnesium binding sites which have a K_{Ca} in the range of 2×10^{7} M^{-1} (Potter & Gergely, 1975). These sites have typically been referred to as the structural sites since they are believed to always be filled with calcium or magnesium in the muscle cell. The N-terminal domain contains the low-affinity calcium-specific binding sites which have a K_{Ca} in the range of 3×10^{5} M^{-1} (Potter & Gergely, 1975; Li et al., 1995). These sites are referred to as the regulatory sites since binding of calcium to these sites regulates muscle contraction.

There have been many studies trying to deduce exactly what the conformational change of TnC is upon binding calcium. It has been suggested, using circular dichroism as a monitor for calcium binding, that the α-helical content of the N-terminal domain of TnC increases upon addition of calcium (Murray & Kay, 1972; Pearlstone et al., 1992a,b; Li et al., 1994; Chandra et al., 1994). In contrast, ^{1}H NMR studies on proteolytic fragments of TnC have revealed that calcium binding to the low-affinity sites results in subtle alterations of the tertiary fold (Evans et al., 1980; Hincke et al., 1981; MacLachlan et al., 1990; Krudy et al., 1992). Hydrophobic interaction chromatography has suggested that the binding of calcium to the TnC low-affinity sites results in the opening of a hydrophobic patch which should be more

‡ The coordinates for the 23 structures and the average NMR structure have been deposited in the Brookhaven Protein Data Bank under the file names 1TNW and 1TNX, respectively.

® Abstract published in *Advance ACS Abstracts,* November 15, 1995.

[1] Abbreviations: TnC, recombinant chicken skeletal troponin C (and unless otherwise stated, TnC will refer to the calcium-saturated state of TnC); NTnC, N-terminal domain (residues 1−90) of chicken skeletal troponin C; NMR, nuclear magnetic resonance; TFE, 2,2,2-trifluoroethanol (and unless otherwise stated, TFE will refer to 15% v/v TFE); NOE, nuclear Overhauser effect; NOESY, nuclear Overhauser enhancement spectroscopy; HCCH-COSY, three-dimensional $^{1}H-^{13}C-^{13}C-^{1}H$ correlation; HSQC, heteronuclear single-quantum coherence; HMQC, heteronuclear multiple-quantum coherence; DQF-COSY, double-quantum-filtered correlated spectroscopy; CSI, chemical shift index; TnI, troponin I; TnT, troponin T.

0006-2960/95/0434-15953$09.00/0 © 1995 American Chemical Society

similar to the two domains of calmodulin than to its own C-terminal domain (Vogel et al., 1983).

A model for the calcium-induced conformational change of the N-terminal domain has been proposed (Herzberg et al., 1986) based on the structure of the C-terminal domain of TnC. The model suggests that when calcium binds to calcium binding sites I and II, the major conformational transition is a movement of the B/C helix pair away from the N/A/D helices to expose a patch of hydrophobic residues that will provide a binding site for other muscle proteins. Several studies, using site-directed mutagenesis (Fujimori et al., 1990; Grabarek et al., 1990; Gusev et al., 1991; Pearlstone et al., 1992a,b), cysteine reactivity in cardiac TnC (Ingraham & Hodges, 1988; Fuchs et al., 1989; Putkey et al., 1993), or NMR studies (Lin et al., 1994; Gagné et al., 1994) have shown that, in general, the model is a good approximation of the actual structure of calcium-saturated TnC in solution. It was shown, however, that while the model may generally be correct, there are problems with the structural details (Pearlstone et al., 1991b; Gagné et al., 1994).

Recently, the 3D solution structures of apo NTnC and calcium-saturated NTnC have been solved (Gagné et al., 1995). These structures confirm previous findings and illustrate not only that the secondary structure of the N-terminal domain remains constant upon calcium binding but that the calcium-saturated N-terminal domain is more open than suggested by the model structure (Gagné et al., 1995). Slupsky et al. (1995a) have shown that the N-terminal domain is involved in the dimerization of TnC at saturating calcium concentrations, and consequently calcium-saturated NTnC should be a dimer in solution. It is therefore important to study TnC in its monomeric form to be sure that the dimer interface does not introduce artifacts into the three-dimensional structure.

There have been a number of questions raised as to the stability of the central helical region of TnC presented in the half-saturated crystal structures. Solution X-ray scattering studies have suggested that TnC is more compact at physiological pH and saturating calcium concentrations (Wang et al., 1987; Hubbard et al., 1988; Heidorn & Trewhella, 1988). This result has been verified using monoclonal antibodies (Strang & Potter, 1990), fluorescence resonance energy transfer (Wang et al., 1993), and site-directed mutagenesis (Reinach & Karlsson, 1988; Gulati et al., 1990, 1993; Dobrowolski et al., 1991; Babu et al., 1993; Ding et al., 1994). Calmodulin, a protein with very similar structural characteristics to TnC, has also been shown to have a flexible central helix (Barbato et al., 1992). With the use of ^{15}N T_2 measurements, it was shown that the central helix of TnC is flexible, but not as flexible as calmodulin (Slupsky et al., 1995a). In order to understand and elucidate the details of the structural change from apo to calcium-saturated TnC in its monomeric form and to study the flexibility of the central helix, we have initiated an NMR study of this protein.

This paper presents the side-chain ^1H, ^{13}C, and ^{15}N assignments and describes the three-dimensional structure of TnC with all four calcium binding sites filled which has been determined using multidimensional heteronuclear nuclear magnetic resonance (NMR) spectroscopy, in the presence of 15% v/v TFE to alter dimerization in favor of monomer. As will be shown, comparison of this calcium-saturated structure with the X-ray crystallographic structure (Herzberg & James, 1988; Satyshur et al., 1988, 1994) of half-saturated skeletal TnC will reveal two major differences. The first difference is an opening of the hydrophobic pocket in the N-domain upon binding calcium, and the second difference involves residues of the interdomain linker where residues 85−94 have conformational heterogeneity resulting in an imprecise spatial relationship between the two domains. The use of 15% v/v TFE as a denaturant of quaternary structure has no effect on the folding of TnC as evidenced by similar structural characteristics between the C-terminal domain of this structure and that of the X-ray crystallographic structure as well as between the N-terminal domain of this structure and that of the NTnC dimer (Gagné et al., 1994). The elucidation of the structure of the calcium-saturated form of TnC is the first step to understanding the link in the signal between TnC and the formation of myosin−actin cross-bridges. These results are also important for understanding the general mechanism of calcium activation in this class of calcium binding proteins.

METHODS

Preparation of Protein. Chicken skeletal troponin C was cloned, expressed, and purified as described in Slupsky et al. (1995a,b). The single cysteine in TnC was reacted with iodoacetamide as described in Slupsky et al. (1995a,b). For NMR spectroscopy, TnC was dissolved to a final concentration of approximately 1.4 mM in a buffer consisting of 150 mM KCl and 15 mM $CaCl_2$ in either 75% H_2O, 10% D_2O, and 15% TFE or 85% D_2O and 15% TFE at a pH of 7.0. The final pH was not corrected for isotope effects.

NMR Spectroscopy. All NMR spectra were acquired at 40 °C on a Varian Unity 600 NMR spectrometer. This temperature was chosen so that dimerization could be minimized without disrupting protein structure (Slupsky et al., 1995a). 2D $^1H-^{15}N$ HSQC and 2D HMQC-J spectra were collected and analyzed as described in Slupsky et al. (1995b). Backbone assignment was carried out as described in Slupsky et al. (1995b).

For side-chain and NOE assignment of TnC, the following spectra were acquired: 3D HCCH-COSY (Ikura et al., 1991), 3D ^{15}N-edited NOESY (75 ms mixing time) (Kay et al., 1989), 3D ^{13}C-edited NOESY (75 ms mixing time) (Ikura et al., 1990), 4D $^{13}C/^{15}N$-edited NOESY (50 ms mixing time) (Kay et al., 1990), 2D $^1H-^1H$ NOESY (75 ms mixing time) (Jeener et al., 1979; Macura & Ernst, 1980), and 2D DQF-COSY (Rance et al., 1983). All spectra were acquired with the proton carrier centered on the water frequency (4.70 ppm), and water suppression was by a low-power (γB_2 = 0.02 kHz) presaturation pulse of approximately 1.5 s duration, or for the HCCH-COSY and ^{13}C-edited NOESY experiments, no form of water suppression was needed. Sweep widths for the proton dimension were 6600 Hz in F_3 and 3600 Hz in F_1 for the HCCH-COSY and ^{13}C-edited NOESY experiments, 8000 Hz in F_4, and 4980 Hz in F_2 for the $^{15}N/^{13}C$-edited NOESY experiment, and 8000 Hz in F_1 and F_2 for the 2D $^1H-^1H$ NOESY and DQF-COSY experiments. For the ^{15}N-edited NOESY and $^{15}N/^{13}C$-edited NOESY experiments, the sweep width in the nitrogen dimension was 1824 Hz centered at 119 ppm. The sweep width of the ^{13}C dimension for the HCCH-COSY, ^{13}C-edited NOESY, and $^{13}C/^{15}N$-edited NOESY experiments was 4224 Hz with the carrier centered at 43 ppm. The HCCH-COSY

experiment was collected with 128 (t_1) × 32 (t_2) × 512 (t_3) complex points with 64 scans per increment, the ^{13}C-edited NOESY experiment was collected with 128 (t_1) × 32 (t_2) × 512 (t_3) complex points with 32 scans per increment, the ^{15}N-edited NOESY experiment was acquired with 128 (t_1) × 32 (t_2) × 512 (t_3) complex points and 64 scans per increment, the 4D ^{15}N/^{13}C-edited NOESY was collected with 12 (t_1) × 32 (t_2) × 12 (t_3) × 512 (t_4) complex points and 48 scans per increment, the 2D ^{1}H−^{1}H NOESY experiment was collected with 512 (t_1) × 2048 (t_2) complex points and 128 scans per increment, and the DQF-COSY experiment was collected with 512 (t_1) × 2048 (t_2) complex points and 128 scans per increment.

For the ^{15}N-edited NOESY experiment, the F_2 dimension was linear predicted such that, after processing, the final size of the spectrum was 1024 (F_3) × 256 (F_1) × 64 (F_2) points. The HCCH-COSY experiment was linear predicted in F_1, and after processing the final size of the spectrum was 1024 (F_3) × 256 (F_1) × 64 (F_2) points. The ^{13}C-edited NOESY experiment was linear predicted in F_1, such that an additional 64 points were added, and in F_2, such that an additional 32 points were added, so that, after zero-filling, the final size of the spectrum was 1024 (F_3) × 512 (F_1) × 64 (F_2) points. The ^{13}C/^{15}N-edited NOESY experiment was linear predicted in F_1, F_2, and F_3, such that after zero-filling the final size of the spectrum was 1024 (F_4) × 128 (F_2) × 32 (F_1) × 32 (F_2). The 2D ^{1}H−^{1}H NOESY experiment was zero-filled in F_1 so that the final size of the spectrum was 2048 (F_1) × 2048 (F_2). The 2D DQF-COSY experiment was zero-filled in F_1 so that the final size of the spectrum was 2048 (F_1) × 2048 (F_2). For all experiments, a postacquisition solvent suppression by convolution of the time-domain data was applied prior to Fourier transformation (Marion et al., 1989b). All 3D and 4D spectra were processed with either a cosine-bell squared or a 60° shifted sine-bell squared weighting function in F_1 and F_2 (and F_3 for the ^{13}C/^{15}N-edited NOESY experiment) and a cosine-bell squared weighting function in F_3 (or F_4 for the ^{13}C/^{15}N-edited NOESY experiment). After Fourier transformation of the F_3 dimension, parts of the spectra without resonances were discarded, reducing the final size to between 50% and 75%. For the 2D NOESY spectrum, both dimensions were processed with a 60° shifted sine-bell squared weighting function, and the 2D DQF-COSY spectrum was processed with a sine-bell function in F_1 and F_2.

Processing of the data sets was accomplished using either the VNMR software (VNMR 4.1A, Varian, Palo Alto, CA) or NMRPIPE (Delaglio et al., NIDDK, NIH, MD, unpublished). When used within VNMR software, extension of the time domain was achieved using the linear prediction algorithm lpfft. Peak-picking was carried out using the interactive graphic-based program PIPP (Garrett et al., 1991).

NOE-Derived Distance Restraints. NOE cross peaks from the 3D ^{15}N- and ^{13}C-edited NOESY experiments, as well as from the 4D ^{15}N/^{13}C-edited NOESY and 2D ^{1}H−^{1}H NOESY experiments, were calibrated for each residue on the basis of known distances. For example, for the ^{15}N-edited NOESY experiment and the ^{15}N/^{13}C-edited NOESY experiments, if the $d_{N\alpha}$ NOE could be obtained, all NOEs for that residue were classified as being stronger or weaker than that NOE. The $d_{N\alpha}$ NOE corresponds to roughly the same distance regardless of the secondary structure (2.70−3.05 Å). Thus, for each residue for which this NOE is found, the upper limits are calibrated according to the equation ucal = $3.05(d_{N\alpha}(i)C)^{1/6}$, where C is a measure of the accuracy of the data (a value of 3 indicates an error of 50% on the NOE) and also accounts for spin diffusion, and the lower limits are calibrated according to the equation lcal = $2.70(d_{N\alpha}(i)/C)^{1/6}$ (S. M. Gagné, personal communication). For each NOE associated with the amide of residue i, the upper bounds and lower bounds will therefore be ucal/NOE$^{1/6}$ and lcal/NOE$^{1/6}$, respectively. The intensity of the $d_{\alpha N}$ NOE is dependent on the type of secondary structure, but is between the broad range of 1.70−3.60 Å. If no $d_{N\alpha}$ NOE is observed for a particular residue, then the $d_{\alpha N}$ NOE is used for calibration of the NOE. If neither the $d_{N\alpha}$ nor the $d_{\alpha N}$ NOEs are observed, then a user-specified maximum and minimum intensity is used for the calibration. Therefore, lower bounds and upper bounds may be obtained for each NOE on a residue per residue basis. For the ^{13}C-edited NOESY, distance restraints were scaled on the basis of known distances of geminal protons or protons on adjacent carbon atoms (the distance between geminal hydrogens is approximately 1.75 Å, and therefore limits of 1.8−2.7 Å may be used as calibration factors; between a methylene hydrogen and degenerate methyl hydrogens, limits of 2.5−2.6 Å may be applied, and between two methylene hydrogens on adjacent carbon atoms, limits of 2.2−3.1 Å may be applied). Aromatic NOE-derived distance restraints are based upon the Hγ to Hδ and Hζ NOE of the aromatic ring (2.47−2.51 Å). For all cases, corrections for degenerate methylene and methyl hydrogens were automatically included to increase the upper bound in the distance restraint by 1 Å. Again, if no calibration NOEs were found for a particular residue, calibration proceeded using the maximum and minimum intensities found in the spectra. During the structure calculations, center averaging was applied to account for nonstereospecifically assigned protons (Wüthrich et al., 1983).

Torsion Angle Restraints. Torsion angle restraints for the ϕ angles were obtained as described in Slupsky et al. (1995b) from an analysis of the 2D HMQC-J experiment. Only those angles for which a low error was obtained in the analysis were used as experimental restraints. For coupling constants less than 9 Hz, inclusion occurred only if a particular type of secondary structure existed, as evidenced by other data such as the CSI or the $d_{N\alpha}/d_{\alpha N}$ ratio, or if, during the early stages of structure calculations, the angles of an ensemble of structures tended to remain in a certain area of the Karplus curve. Most ϕ angles were given errors of ±10° except for those near the top of the Karplus curve (>9 Hz) and for those which consistently violated NOE distance restraints. ψ angles were obtained from an analysis of the $d_{N\alpha}/d_{\alpha N}$ ratio according to Gagné et al. (1994). For ratios less than 1, ψ = 120 ± 100°, and for ratios greater than 1, ψ = −30 ± 110°.

Structure Calculations. Three-dimensional structures were computed from experimental restraints using a simulated annealing protocol (Nilges et al., 1988b,c) with the program X-PLOR 3.1 (Brünger, 1992). The initial structure used was the model structure for calcium-saturated TnC (Herzberg et al., 1986). Upon completion of the structure calculations using only simulated annealing, the TnC structure was generated from a random array of coordinates using the hybrid distance geometry/simulated annealing protocol (Nilges et al., 1988a; Kuszewski et al., 1992) to ensure no

bias was placed on the final structure by the starting coordinates. The target function contained only quadratic harmonic potential terms for covalent geometry (bonds, angles, planes, and chirality), square well quadratic potentials for the torsion angle restraints, a soft-square quadratic potential (simulated annealing) or square well quadratic potential (hybrid distance geometry/dynamical simulated annealing protocol) for the experimental distance restraints, and a quartic van der Waals repulsion term for the nonbonded contacts (the X-PLOR F_{repel} function was set to 0.75). Force constants for the NOE-derived distance restraints were set to 50 kcal·mol^{-1}·Å^{-2}, and the dihedral angle restraints were initialized at 5 kcal·mol^{-1}·rad^{-2} during the high-temperature dynamics and increased to 200 kcal·mol^{-1}·rad^{-2} during the annealing stage. Annealing proceeded stepwise from 1000 to 100 K in decrements of 50 K. The force constant on the repulsive term was increased stepwise to 4.0 kcal·mol^{-1}·Å^{-4} and was maintained until the end of the penultimate energy minimization step, which consisted of 500 cycles of Powell minimization with the van der Waals hard-sphere radii set to 0.8 times the CHARMM values (Brooks et al., 1983). The final energy minimization step employed the 6−12 Lennard-Jones potential.

The final structure calculations were based upon 2106 NOE-determined distance restraints, with 505 sequential, 321 medium range (between one and five residues apart), 284 long range (more than five residues apart), and 996 intraresidue, and 121 ϕ restraints and 76 ψ restraints.

RESULTS AND DISCUSSION

Side-Chain Assignment. The ^{1}H, ^{13}C, and ^{15}N NMR chemical shifts of skeletal troponin C were assigned using double and triple resonance three-dimensional NMR experiments on samples of uniformly ^{15}N- and ^{15}N/^{13}C-labeled protein (see Methods section for experimental details). Backbone assignment of calcium-saturated TnC was accomplished as described in Slupsky et al. (1995b). Side-chain assignment involved the combined analysis of 3D HCCH-COSY, ^{13}C-edited NOESY, and ^{15}N-edited NOESY and 2D ^{1}H−^{1}H DQF-COSY and NOESY experiments. The first step in side-chain assignment involved identifying $^{13}C_\alpha$ and $^1H_\alpha$ resonance chemical shifts on an HCCH-COSY experiment and correlating these with the $^1H_\beta$ resonance. Each plane on the HCCH-COSY spectrum was then examined to find the symmetrically related $^{13}C_\beta/^1H_\beta$ peak correlating the $^1H_\beta$ resonance to the $^1H_\alpha$ resonance. This procedure was continued along the side chain finding symmetrically related peaks correlating ^{1}H resonances and their attached ^{13}C frequencies with ^{1}H resonances on adjacent carbon atoms. Figure 1 illustrates an HCCH-COSY spectrum where the assignment of T72 and I130 is shown. Assignment of isoleucine 130 was initiated by finding the ^{13}C plane correlating the $^{13}C_\beta/^1H_\beta$ resonance with the $^1H_\alpha$ and γ-methyl and methylene protons. The HCCH-COSY spectrum was subsequently surveyed to find the symmetric peaks from the $^{13}C_\gamma/^1H_3C_\gamma$ to the $^1H_\beta$ (to obtain the ^{13}C assignment of the γ-methyl carbon) and the $^{13}C_\gamma/^1H_2C_\gamma$ to the $^1H_\beta$ and to the $^1H_3C_\delta$ protons. For assignment of the $^{13}C_\delta$, the symmetric peak correlating $^{13}C_\delta/^1H_3C_\delta$ to the γ-methylene protons were found. This figure illustrates the ease at which the side-chain assignment was obtained. Also shown in Figure 1 is the assignment of T72 of the N-terminal domain. Assignment of all residues was verified by finding

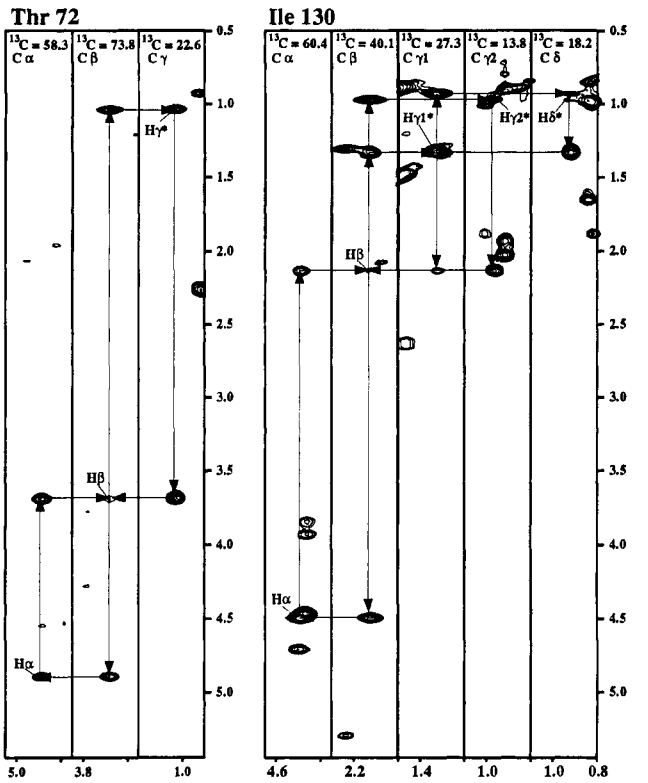

FIGURE 1: Side-chain assignment of threonine 72 located in the N-terminal domain of TnC and isoleucine 130 located in the C-terminal domain of TnC. Shown are strips taken from different ^{13}C planes (^{13}C frequency is indicated at the top of the strip) of the HCCH-COSY spectrum illustrating how side-chain assignment was accomplished using this experiment.

similar peaks in the ^{13}C-edited NOESY spectrum. Assignment of the aromatic rings of TnC (11 phenylalanine residues) was done by a combination of 2D DQF-COSY and NOESY experiments in D_2O, where connectivities through the ring were found on the DQF-COSY spectrum and assignment to a particular residue was made from observation of an NOE from the δ-ring protons to the $^1H_\beta$ protons. Assignment of side-chain amide resonances (from asparagine and glutamine residues) was accomplished using the ^{15}N-edited NOESY experiment, where NOEs from the amide to H_β or H_γ protons were found. The complete side-chain assignment (^{1}H, ^{13}C, and ^{15}N) of calcium-saturated TnC is given in the supporting information.

Quality of TnC Structure. The three-dimensional structure of calcium-saturated skeletal TnC was determined using a simulated annealing protocol from a total of 2282 NMR-derived restraints (Nilges et al., 1988a−c). The structures all satisfy the distance restraints with no violations greater than 0.35 Å and no dihedral violations greater than 5°. Details of how the distance and angular information were obtained may be found in the Methods section. A superposition of 23 NMR-derived structures is shown in Figure 2, and the structural statistics are given in Table 1. Residue-based rms deviations for these structures are shown in Figure 3, and angular order parameters are shown in Figure 4. As shown in Table 1, the NMR structures exhibit good covalent geometries (as indicated by the low rms deviations from idealized values for bonds, angles, and impropers, as well as low values for the dihedral, NOE, van der Waals, and total energies calculated with the use of a van der Waals repulsion term of 0.75). In addition, the large negative

Table 1[a]

Rms Deviations from Idealized Values	
bonds (Å)	0.004 ± 0.000
angles (deg)	0.403 ± 0.011
impropers (deg)	0.308 ± 0.011
X-PLOR Energies (kcal mol^{-1})	
E_{total}	279.4 ± 23.6
E_{vdw}[b]	66.4 ± 17.6
$E_{L\text{-}J}$	−650.9 ± 21.4
E_{edih}	3.0 ± 0.6
E_{NOE}	40.3 ± 7.1

[a] The values reported are for the ensemble of 23 X-PLOR structures generated from the simulated annealing protocol as described in the X-PLOR 3.1 manual (Brünger, 1992). [b] The X-PLOR F_{repel} function was used to simulate the van der Waals interactions with atomic radii set to 0.75 times their CHARMM (Brooks et al., 1983) values. E_{vdw} and E_{total} reflect the use of this approximation. In the final minimization step of simulated annealing, a 6−12 Lennard-Jones potential was applied, and the energy is as shown with the variable $E_{L\text{-}J}$ (see Methods section for more details).

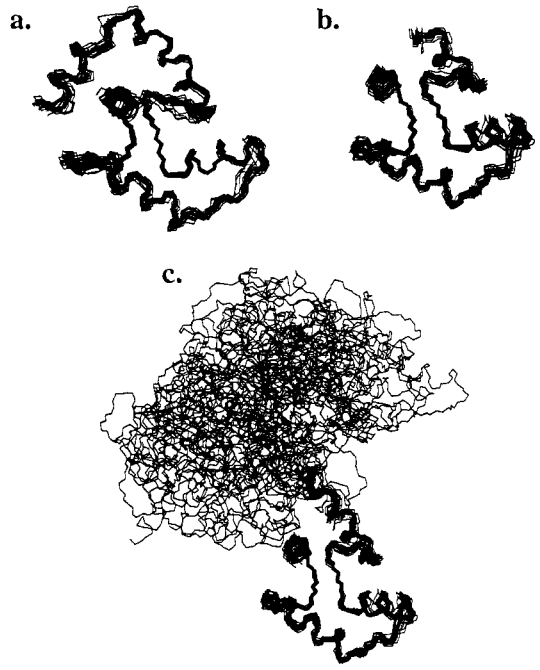

FIGURE 2: Superposition of 23 X-PLOR-generated structures for calcium-saturated recombinant chicken skeletal troponin C. (a) Superposition of residues 10−80 of the N-terminal domain (residues 1−90) onto the mean atomic coordinates. Shown are residues 5−83. (b) Superposition of residues 98−155 of the C-terminal domain (residues 91−162) onto the mean atomic coordinates. Shown are residues 95−158. (C) Same as (B), but showing residues 5−158.

Lennard-Jones van der Waals energy indicates that there are no bad nonbonded contacts.

Shown in Figure 2a,b is a superposition of the 23 structures of the N-terminal and C-terminal domains onto the N-terminal and C-terminal domain average minimized structures, respectively. As can be seen, most of the backbone atoms in the N- and C-terminal domains exhibit good structural convergence. The atomic rms distribution about the mean coordinate positions for residues 10−80 is 0.66 ± 0.17 Å for backbone atoms and 1.07 ± 0.14 Å for all heavy atoms and for residues 98−155 is 0.69 ± 0.18 Å for backbone atoms and 1.17 ± 0.16 Å for all heavy atoms. The structures of the backbone and the hydrophobic core side-chain residues are therefore well-defined by the NMR data except for the first four residues of the N-terminal

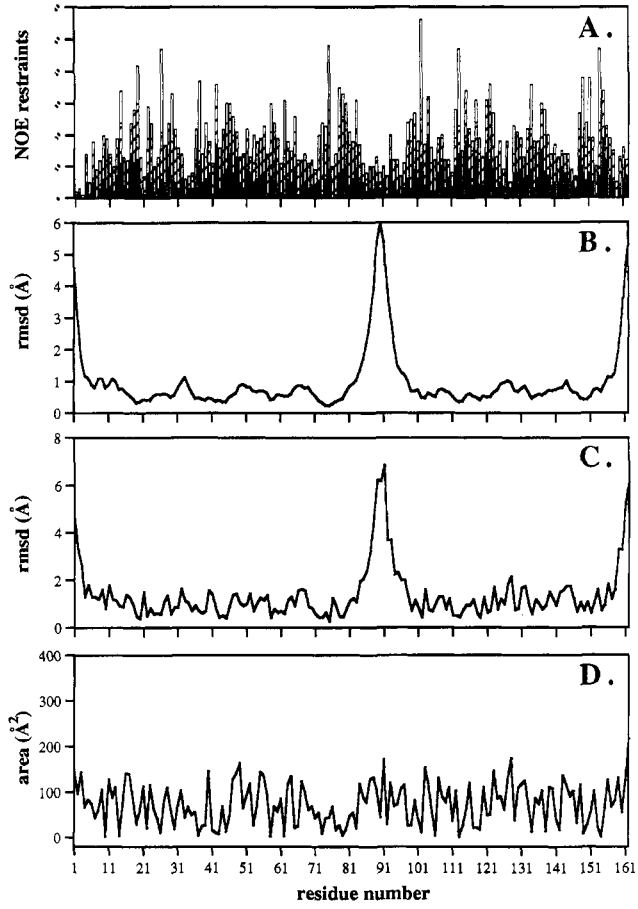

FIGURE 3: (A) Distributions of NOEs that were used in the structure calculations. The height reflects the total number of NOE-derived restraints for each residue. Intraresidue, sequential plus medium-range, and long-range NOEs are indicated by the black, hatched, and white portions of the box. (B, C) Atomic rms deviations (Å) of the 23 individual structures about the mean structure for (B) backbone atoms (N, Cα, C′) and (C) heavy atoms. (D) Residue-based solvent-accessible surface area in Å^2.

domain, the last five residues of the C-terminal domain, and the linker region between the two domains (residues 85−94). ^{15}N T_2 NMR relaxation data (Slupsky et al., 1995a) has revealed that residues 86−88, as well as the last two residues at the C-terminus, are highly flexible, indicating that these regions of the protein experience conformational diversity. As a result of the increased mobility of residues 86−88, there is significant structural heterogeneity resulting in a spatial relationship between the two domains which is ill-defined (Figure 2c).

Figure 3 illustrates the compilation of statistics from each domain which have been concatenated to generate statistics for the whole molecule. The number of NOE restraints the rms deviations from the average structure of the backbone and heavy atoms, along with the variation in surface accessibility on a residue per residue basis, are shown. On average, 13 NOE restraints per residue were used in the structure calculations. Areas which lacked NOE restraints (residues 1−4, 33−35, 85−94, and 158−162) in general were the least well ordered, as shown in Figure 3B,C. The rmsd's indicate that the overall structure is very well defined (except for the ends of the molecule and the central region where conformational heterogeneity exists), with the regular secondary structure elements (α-helices and β-sheets) extremely well defined.

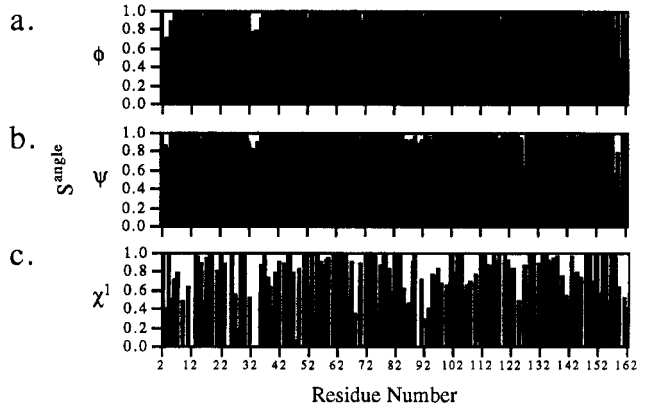

FIGURE 4: Order parameters for (a) ϕ, (b) ψ, and (c) χ_1 angles for the 23 structures of calcium-saturated skeletal TnC as a function of residue number.

The convergence of the TnC structures was also analyzed by obtaining the angular order parameter of the ϕ, ψ, and χ^1 torsion angles as a function of residue number according to the method of Hyberts et al. (1992). The angular order parameter is a measure of the deviation of a particular torsion angle. If the angular order parameter has a value of 1, then the angle is identical in all structures. If the angular order parameter has a value of 0, then the angle deviates in a random manner, and thus a disordered structure is inferred. A value of $S = 0.99$ corresponds to a standard deviation of $\pm 7.5°$, a value of $S = 0.95$ corresponds to a standard deviation of $\pm 17°$, and a value of $S = 0.9$ corresponds to a standard deviation of $\pm 24°$. Thus, the order parameter is related to the standard deviation in a logarithmic manner (Hyberts et al., 1992). It is important to note that low values of the angular order parameter for residues that have symmetrically branched side chains, such as Asp, Glu, Leu, Phe, Tyr, and Val, may be obtained but may not always result from poor convergence (Meadows et al., 1993). A 180° rotation of the side-chain atoms may produce two equally favorable yet out-of-phase populations with a near zero angular order parameter (Meadows et al., 1993).

The order parameters shown in Figure 4 indicate that the overall structure, in terms of torsion angles, is very well defined. Angular order parameters for the ϕ and ψ backbone dihedrals had mean values of 0.98 ± 0.1 and 0.97 ± 0.1 (for residues 5−158), respectively, indicating very good convergence for these torsional angles. Residues with low angular order parameters (<0.90) are residues at the beginning and ends of the molecule (residues 1, 2, 3, 4, 5, 158, 159, 160), as well as a few others (33, 34, 35, 71, 87, 90, 92, 95, 119, 127, 128). Residues at the ends of the molecule tend to be disordered, and thus low angular order parameters for these residues are to be expected. Residues 87, 90, 92, and 95 are present in the region of TnC associated with conformational heterogeneity. The low angular order parameters in this region may be because of too few NMR restraints. The low angular order parameters obtained for residues 33, 34, 35, 71, 119, 127, and 128, which are all glycines (except for residues 127 and 128), are most likely due to the lack of experimental restraints (see Figure 3).

Figure 5 illustrates the individual superimposed helices N, A, B, C, D, E, F, G, and H, as well as the β-sheet regions in the N- and C-terminal domains together with some of the well-defined side-chain residues. As is evident from Figures 3−5, the high definition of the structures is not confined

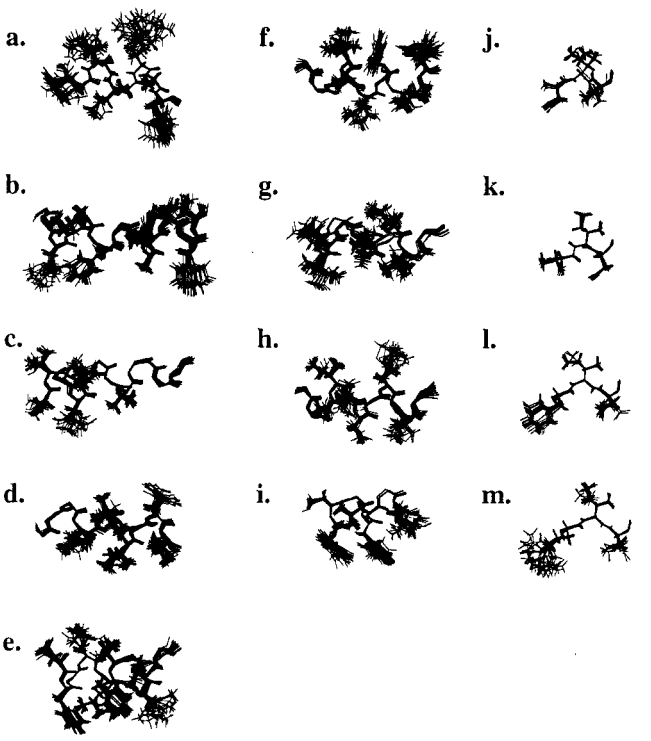

FIGURE 5: Superposition of the secondary structure elements of TnC with some side chains: (a) N-helix (residues 5−13) illustrating all side-chain residues (backbone rmsd = 0.17 ± 0.08); (b) helix A (residues 16−30) illustrating the side chains of residues 18, 19, 20, 22, 24, 25, 26, 27, 29, and 30 (backbone rmsd = 0.25 ± 0.08); (c) helix B (residues 38−49) illustrating the side chains of residues 38, 39, 41, 42, and 45 (backbone rmsd = 0.21 ± 0.07); (d) helix C (residues 55−65) illustrating the side chains of residues 58, 60, 61, 62, 64, and 65 (backbone rmsd = 0.26 ± 0.12); (e) helix D (residues 74−84) illustrating the side chains of residues 74, 75, 77, 78, 79, 80, 82, and 83 (backbone rmsd = 0.17 ± 0.06); (f) helix E (residues 95−105) illustrating the side chains of residues 98, 99, 100, 102, 104, and 105 (backbone rmsd = 0.25 ± 0.06); (g) helix F (residues 114−124) illustrating the side chains of residues 115, 116, 118, 121, and 122 (backbone rmsd = 0.26 ± 0.13); (h) helix G (residues 131−141) illustrating the side chains of residues 133, 134, 135, 136, 138, and 140 (backbone rmsd = 0.24 ± 0.06); (i) helix H (residues 150−158) illustrating the side chains of residues 151, 152, 154, 155, and 157 (backbone rmsd = 0.15 ± 0.05); (j) β-sheet in calcium binding site I (residues 36−38); (k) β-sheet in calcium binding site II (residues 72−74) (backbone rmsd for antiparallel sheet = 0.20 ± 0.09); (l) β-sheet in calcium binding site III (residues 112−114); (m) β-sheet in calcium binding site IV (residues 148−150) (backbone rmsd for antiparallel sheet = 0.13 ± 0.04).

solely to the backbone. Many of the side chains exhibit atomic rms deviations with respect to the mean of less than 1 Å and order parameters close to 1. Almost all of the ill-defined side chains, however, exhibit a larger surface accessibility in the minimized mean structure when compared to the well-defined side chains, indicating greater solvent exposure for these side chains. Those side chains which have a χ^1 angular order parameter of less than 0.8 are M3, D5, Q6, Q7, E9, R11, E16, D27, M28, D32, S38, T39, K40, E41, R47, M48, N52, T54, D66, D68, E76, M81, Q85, M86, K87, K91, K93, S94, E95, E96, L98, N100, R103, D106, K107, N108, D110, T125, H128, E131, K139, D140, S141, D142, N144, N145, D146, D150, E153, E156, E159, V161, and Q162. As can be observed, most of the residues with ill-defined side chains are charged or polar. M3 and V161 are hydrophobic residues present at the ends of the molecule, and thus it is likely that their side chains exhibit conforma-

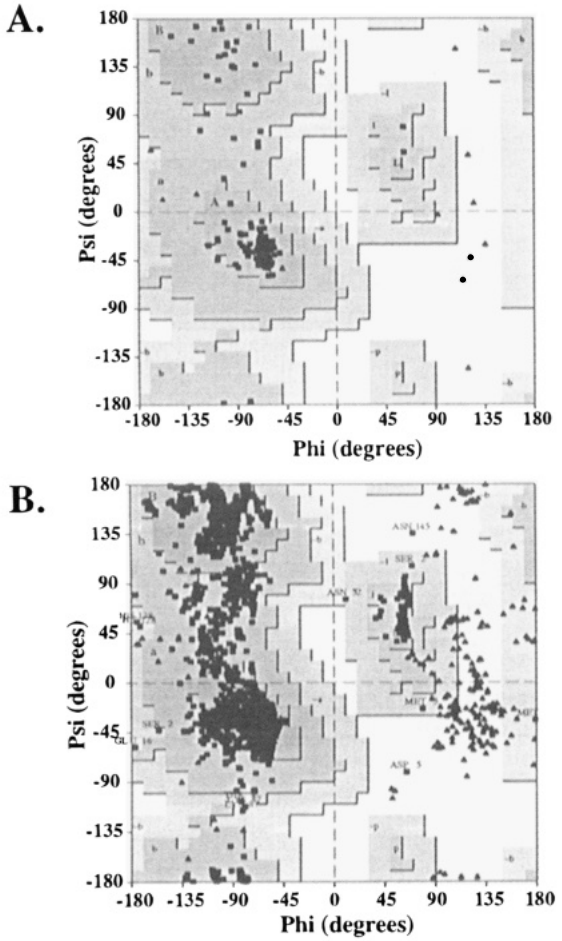

FIGURE 6: Ramachandran ϕ, ψ plot for (A) the average structures of the N- and C-terminal domains and (B) all 23 structures. Triangles represent glycine residues, whereas all other residues are represented by squares. The plot was generated using the program PROCHECK.

tional heterogeneity. Two of the methionines (28 and 48) exhibit greater solvent-accessible surface areas (110 and 140.8 Å^2, respectively). Methionines 81 and 86, and leucine 98, however, have somewhat buried side chains (solvent-accessible surface areas of 47.4, 78.3, and 27.5 Å^2, respectively) and χ_1 angular order parameters of approximately 0.55. Methionine low angular order parameters may be due simply to the fact that, because of the presence of the sulfur atom, there is little enthalpic discrimination among the possible χ_3 torsion angles (Gellman, 1991). This suggests that there is substantial flexibility in the methionine side chain which may result in a low angular order parameter for the χ_1 torsion angle.

Figure 6 shows a Ramachandran plot of the ϕ and ψ angles for the average structure, as well as all 23 structures. For the average structure, all backbone torsion angles of non-glycine residues fall in the allowed regions of the Ramachandran ϕ, ψ plot (glycine residues are indicated by the triangular markers, and all other residues are indicated by the square markers). The two square markers present in the allowed positive ϕ region are alanine 109 and asparagine 145, which will be discussed below. For all 23 structures, 89% of the ϕ, ψ angles fall within the most favored region of the Ramachandran plot (marked as A, B, L, and P), 11% fall within the additionally allowed regions (marked as a, b, and l), and 0.3% fall within the generously allowed regions (marked as ~a, ~b, ~l, and ~p). Those residues present in the generously allowed regions and disallowed regions are indicated. Out of 3726 residues in the 23 structures, there are only two residues which are within the disallowed region, namely, aspartic acid 5 and asparagine 145. Aspartic acid 5 is a residue near the N-terminal region of the protein and, as indicated above, exhibits a lower angular order parameter. Asparagine 145 is a residue in the C-terminal domain calcium binding loop. This residue and the equivalent residue in calcium binding site III (alanine 109) are involved in a type III Asx turn (ϕ, ψ angles of approximately 60°, 30°) as was observed in the crystal structure for these residues (Herzberg & James, 1985). The equivalent residues in the N-terminal domain are glycines (33 and 69). The angular order parameter for asparagine 145 is >0.9 for the ϕ and ψ angles, and therefore, in general, this residue is well-defined; however, for one structure a ψ angle of 135° was found. This value for the ψ angle is within the error limits put on the residue for the angle 120 ± 100°. The backbone rmsd for residues in the calcium binding loop regions are generally slightly higher than for other, well-defined regions (in terms of secondary structure) of the molecule, which could account for the deviation in one of the structures.

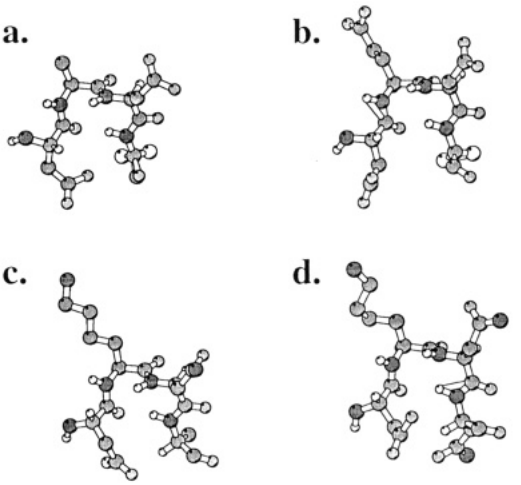

FIGURE 7: Four type I turn conformations found at the beginning of each of the calcium binding loops shown from the minimized mean structure of TnC: (a) calcium binding loop I (residues 30−33), (b) calcium binding loop II (residues 66−69), (c) calcium binding loop III (residues 106−109), and (d) calcium binding loop IV (residues 142−145). This figure was prepared using MOLSCRIPT (Kraulis, 1991).

Description of the Structure. The structure of calcium-saturated TnC reveals a protein consisting of two domains with a total of nine helices [N (5−13), A (16−29), B (39−48), C (55−64), and D (75−84) in the N-terminal domain and E (95−105), F (116−124), G (131−141), and H (151−158) in the C-terminal domain] and two antiparallel β-sheet regions (residues 36−38 and 72−74 forming an antiparallel β-sheet in the N-terminal domain and residues 112−114 and 148−150 forming an antiparallel β-sheet in the C-terminal domain) forming four helix−loop−helix calcium binding sites. The four calcium binding loop regions start with a type I turn (Figure 7) as evidenced by NOE data (Slupsky et al., 1995b) and ϕ, ψ angles, which consist of residues 30−41 (site I), 66−77 (site II), 106−117 (site III), and 142−153 (site IV). Helices A and B as well as C and D in the N-terminal domain and helices E and F as well as G and H in the C-terminal domain form the helices flanking the calcium binding loops (the so-called Ca^{2+} binding EF-hands).

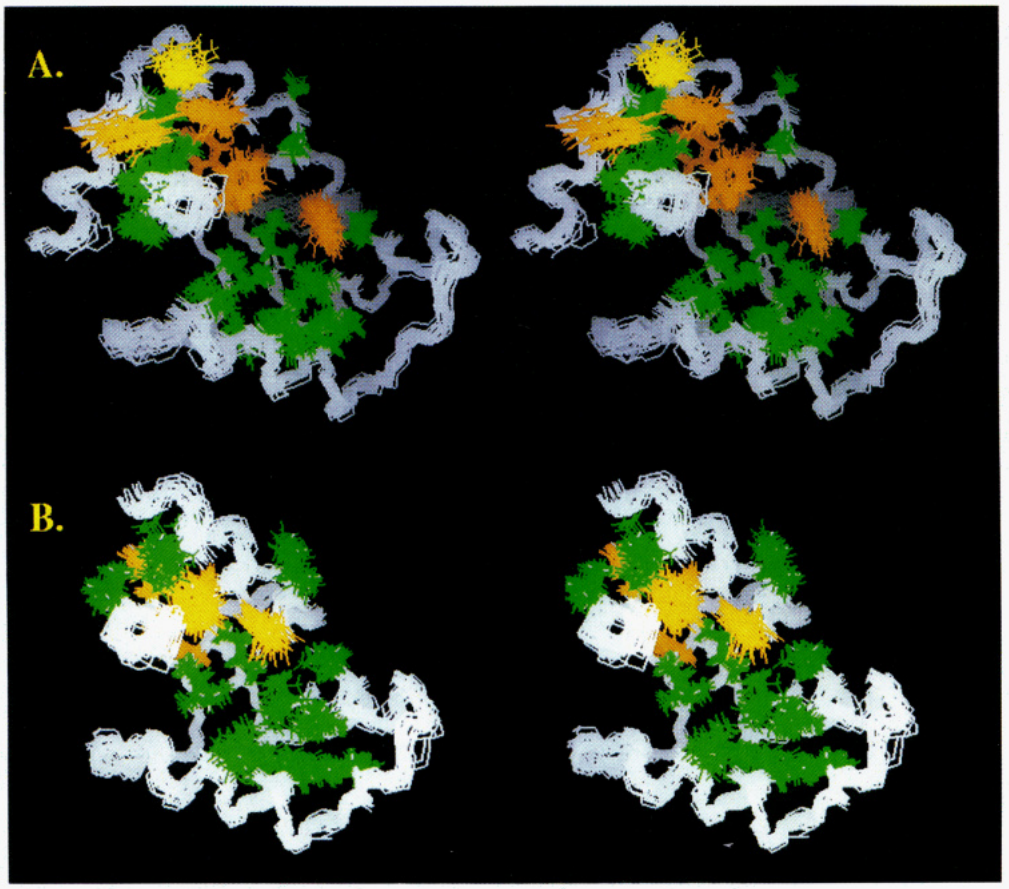

FIGURE 8: Stereoviews of the backbone and selected side-chain residues of 23 superimposed NMR-derived structures of (A) the N-terminal domain of TnC and (B) the C-terminal domain of TnC. This figure was prepared using BIOSYM INSIGHT II software.

The N-helix (residues 5−13) wraps around helix D, making several contacts between the side-chain residues of both helices. (Several NOEs are observed between glutamine 6, glutamine 7, alanine 10, and phenylalanine 13 of the N-helix with valine 80 and valine 83 of helix D.) Residues 85−94 are ill-defined by the present data and appear to be disordered. A disordered central region for TnC is supported by the observation of differential line widths for the two domains and increased mobility of residues in the central region as evidenced by ^{15}N T_2 data (Slupsky et al., 1995a).

Figure 8 illustrates stereoviews of the ensemble of NMR-derived structures with the well-defined hydrophobic core side chains appropriately colored [hydrophobic residues (alanine, valine, leucine, and isoleucine) are green, phenylalanine residues are brown, and methionine residues are yellow]. The figure illustrates five phenylalanine residues present in the hydrophobic pocket of the N-terminal domain (residues 22, 26, 29, 75, and 78), and four in the C-terminal domain (residues 102, 105, 151, and 154). Shown as well are several isoleucine, leucine, and valine residues. The core of the hydrophobic pocket arises from residues primarily from the amphipathic helices comprising the EF-hand calcium binding loops as well as residues from the calcium binding loop itself. As can be observed from the figure, the hydrophobic pocket present in the N-terminal domain appears to have a larger surface area than the hydrophobic pocket of the C-terminal domain.

The larger exposed hydrophobic surface area of the N-terminal domain as compared to the C-terminal domain may also be observed in Figure 9B,C where the structures of the minimized average N-terminal and C-terminal domains are illustrated in CPK format. For the average structure, the total exposed nonpolar accessible surface area is 3316.2 Å^2 for the N-terminal domain and 2683.5 Å^2 for the C-terminal domain (as determined using the in-house program VADAR; D. S. Wishart, L. Willard, and B. D. Sykes, unpublished). All atoms from hydrophobic residues are shown in green, whereas all other atoms are shown in white. Also shown in Figure 9A is the CPK format of the crystal apo N-terminal domain calcium binding sites. This figure illustrates a substantial opening of the N-terminal domain upon binding of calcium to expose a large hydrophobic area, which appears to be much larger than that observed for the C-terminal domain. This large exposed hydrophobic area is most likely the cause of the calcium-induced dimerization characterized in Slupsky et al. (1995a), which involves the hydrophobic patch of one TnC N-terminal domain interacting with the N-terminal domain hydrophobic patch of a symmetrically related TnC molecule.

Comparison of the NMR-Derived Structure of Calcium-Saturated TnC to Other Structures. EF-hand calcium binding domains are present in a variety of proteins with differing functions. One of the most closely related proteins to TnC, in terms of structure, is calmodulin. The elements of secondary structure of the two proteins have been shown, upon alignment of the calcium binding loops, to be homologous to one another (Slupsky et al., 1995b) and to the half-saturated X-ray crystallographic form of TnC (Slupsky et al., 1995b). There have been many studies of both calmodulin and TnC in terms of structure. Until now, however, the calcium-saturated structure of TnC had not been solved. Now that this structure is complete, it appears that both TnC

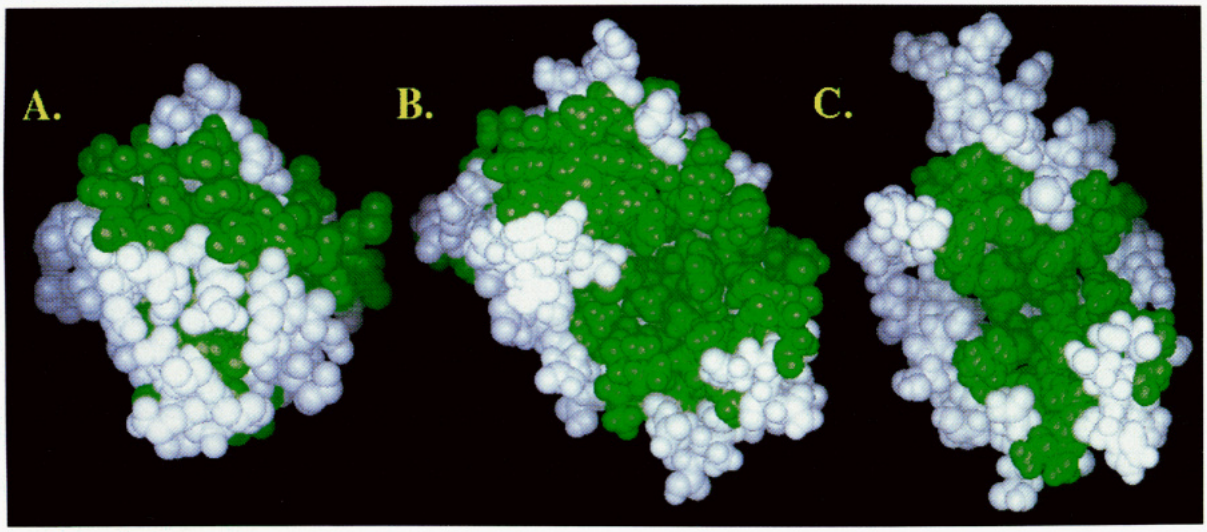

FIGURE 9: CPK illustrations of (A) the X-ray crystal structure of the apo N-terminal domain of turkey TnC [from Herzberg and James (1988)], (B) the average minimized NMR-derived structure of the calcium-saturated N-terminal domain of recombinant chicken skeletal TnC, and (C) the average minimized NMR-derived structure of the calcium-saturated C-terminal domain of recombinant chicken skeletal TnC. Shown in green are all hydrophobic side-chain atoms and in white are all other atoms. The difference between chicken cloned and turkey skeletal troponin C's is the substitution of an alanine for proline in position 1, isoleucine for threonine at position 130, and aspartic acid for glutamic acid at position 133. This figure was prepared using BIOSYM INSIGHT II software.

and calmodulin share more similarities than was originally thought. Figure 10 illustrates ribbon diagrams of the NMR-derived calcium-saturated structure of TnC in comparison with half-saturated TnC (X-ray crystal structure) (Herzberg & James, 1988), the model structure based on the C-terminal domain of TnC (Herzberg & James, 1986), the structure of calcium-saturated NTnC (Gagné et al., 1995), and calcium-saturated calmodulin (Chattopadhyaya et al., 1994).

Shown in Figure 10B are the structures of the C-terminal domains of the crystal structure of TnC, the average NMR structure, and calmodulin. The rmsd for backbone atoms comprising residues 98−155 is 1.22 Å between the average minimized NMR structure and the crystal structure of TnC and 1.67 Å between residues 85−142 of calmodulin and residues 98−155 of the average minimized structure of TnC. The NMR-derived structure of the C-terminal domain of TnC therefore most closely resembles the crystal structure of TnC. Several studies confirm that the C-terminal domain of calmodulin behaves differently from the C-terminal domain of TnC. One study of proteolytic fragments of calmodulin and TnC revealed that the C-terminal domain of calmodulin, but not TnC, could interact with a hydrophobic interaction chromatography column (Vogel et al., 1983).

The conformation of the N-terminal domain of TnC is markedly different from the C-terminal domain, the X-ray structure, or the model structure but is similar to the N-terminal domain of calmodulin and the calcium-saturated structure of NTnC. Figure 10A illustrates the different structures of the N-terminal domain. The rmsd for backbone atoms comprising residues 5−83 is 5.45 Å between the apo X-ray structure of TnC and the average minimized calcium-saturated structure of TnC and 1.06 Å upon alignment of only residues 5−30 and 75−83. Therefore, the major difference between the X-ray structure of half-saturated TnC and the NMR structure of calcium-saturated TnC is as was predicted by Herzberg et al. (1986), which is the movement of helices B and C away from helices N, A, and D. The rmsd for backbone atoms comprising residues 5−83 of TnC and NTnC is 1.28 Å and between residues 6−73 of calmodulin and residues 16−83 of TnC is 1.25 Å. These rmsd values suggest that the structure of the isolated N-terminal domain of TnC in its dimeric calcium-saturated form and the structure of the N-terminal domain of calcium-saturated calmodulin bear a striking resemblance to the N-terminal domain of calcium-saturated TnC. A comparison of the structure of the N-terminal domain of calcium-saturated TnC with that of the model of calcium-saturated TnC reveals an rmsd of 2.25 Å, suggesting that although the model structure, in general, predicts what the global change is when TnC binds calcium, the actual structure is somewhat different. The model predicts that the change should be similar to the calcium-saturated structure of the C-terminal domain of TnC; however, the actual structure of the calcium-saturated N-terminal domain of TnC is more similar to the calcium-saturated N-terminal domain of calmodulin than to the calcium-saturated C-terminal domain of TnC. Pearlstone et al. (1991b) also suggested that the actual structure may be somewhat different than what was predicted.

Table 2 is a summary of the interhelical angles comparing calcium-saturated TnC, calcium-saturated calmodulin (Babu et al., 1988; Chattopadhyaya et al., 1994), half-saturated TnC (X-ray crystal structure) (Herzberg & James, 1988; Satyshur et al., 1988, 1994), and the Herzberg−James model for the N-domain of calcium-saturated TnC (Herzberg et al., 1986). The conformation of the C-terminal domain of the NMR structure resembles both the X-ray crystal structure and calmodulin in terms of the interhelical angles, except for the H to G interhelical angle. In calmodulin, the slightly smaller H to G interhelical angle indicates a slightly more open C-terminal domain, accounting for the higher rmsd between TnC and calmodulin, and the apparent more open structure of calmodulin versus TnC (Vogel et al., 1983).

The conformation of the N-terminal calcium-saturated domain of TnC resembles that of calmodulin in terms of interhelical angles but appears to be more open upon comparison with the model structure (a decrease in the interhelical angle of B to A, C to N, or D to C indicates a

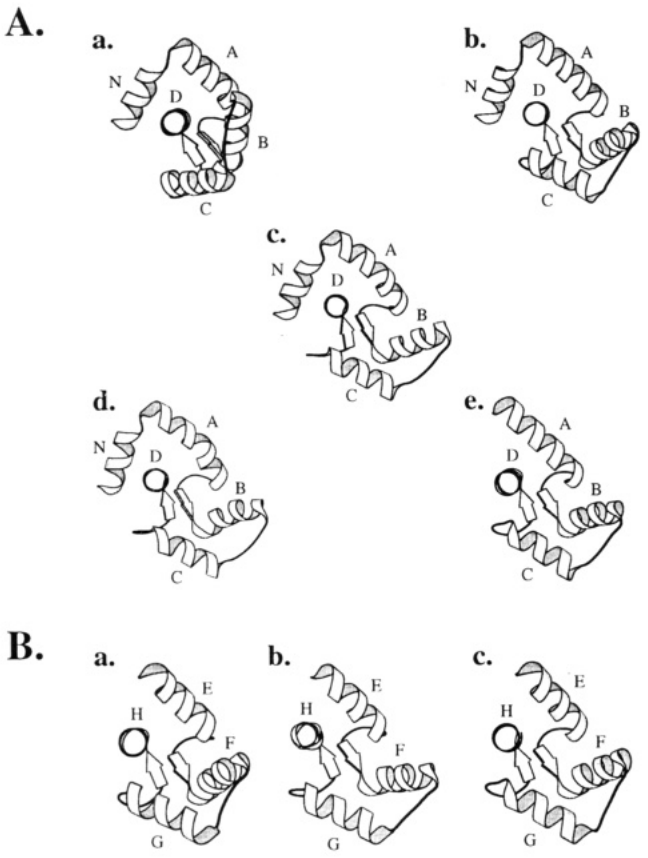

FIGURE 10: Ribbon plots depicting (A) the N-terminal domain of (a) the half-saturated X-ray structure (residues 5−83) (Herzberg & James, 1988) (monomer), (b) the Herzberg−Moult−James model structure of TnC (residues 5−83) (monomer) (Herzberg et al., 1986), (c) the average calcium-saturated NMR structure (residues 5−83) (monomer), (d) the average calcium-saturated NTnC structure (residues 5−83) (dimer) (Gagné et al., 1995), and (e) calcium-saturated calmodulin (residues 16−73) (monomer) (Chattopadhyaya et al., 1994) and (B) the C-terminal domain of (a) the half-saturated X-ray structure (residues 98−155) (monomer) (Herzberg & James, 1988), (b) the average calcium-saturated NMR structure (residues 98−155) (monomer), and (c) calcium-saturated calmodulin (residues 85−142) (monomer) (Chattopadhyaya et al., 1994). The structures are oriented such that, for the N-terminal domain, helix D is coming out of the page toward the viewer and, for the C-terminal domain, helix H is is coming out of the page toward the viewer. On each of the structures the helices are designated by capital letters. The ribbons were generated using MOLSCRIPT (Kraulis, 1991).

Table 2: Comparison of Interhelical Angles[a]

	N-Domain					
coordinates	B to A	C to N	C to B	D to A	D to B	D to C
crystal	131.7	132.9	131.5	117.8	47.8	144.7
model	98.6	97.4	127.1	113.1	34.2	111.3
calmodulin	85.1	n/a	113.3	107.7	40.3	86.8
av NMR	79.2	87.2	117.6	108.8	57.0	80.8
	C-Domain					
coordinates	F to E	G to E	G to F	H to E	H to F	H to G
crystal	107.2	128.8	123.2	118.6	35.2	108.2
calmodulin	101.3	146.6	112.1	119.4	40.7	87.9
av NMR	97.8	135.0	127.0	112.5	25.6	108.0

[a] As determined by the programs bestfits and interhx provided in the Ribbons 2.0 package (Carson, 1987).

more open structure) and very much more open upon comparison with the crystal apo N-terminal domain. The interhelical angles presented here for calcium-saturated TnC are similar to those obtained for the NTnC dimer (Gagné et al., 1994). This indicates that the structures of the calcium-saturated NTnC dimer and the TnC monomer are similar. These results suggest that dimerization has little effect on the tertiary structure of TnC and that the C-terminal domain of TnC has no effect on the structure of the N-terminal domain of TnC. These results also indicate that studies involving fragments of the N-terminal and C-terminal domains of TnC are good approximations of the whole molecule.

It is clear from these data that 15% v/v TFE has little effect on tertiary structure, thus reinforcing the use of TFE as a general perturbant of quaternary structure. As well, dimerization does not appear to have a major effect on the tertiary structure of TnC, as the rmsd between NTnC and the N-terminal domain of TnC is low. Both structures therefore validate one another and most likely represent the structure of the N-terminal domain of TnC when bound to TnI. Further, since TFE is a small molecule, the binding of some TFE to TnC would result in very little increase in molecular weight of TnC, in contrast to the detergent CHAPS, making its general use as a denaturant of quaternary structure applicable.

Shown here, for the first time, is the structure of calcium-saturated TnC, which demonstrates two aspects of its function making it different from most other similar calcium binding proteins. First, upon calcium binding, the N-domain hydrophobic pocket opens up to produce a hydrophobic area which is more exposed than in the absence of calcium. This large exposed hydrophobic area is the reason for dimerization of TnC and is what would enhance the interaction between the N-terminal domain of TnC and the C-terminal domain of troponin I in the muscle filament. Second, the flexible linker between the two domains allows TnC to explore a variety of orientations with respect to the C-terminal domain of TnC while the C-terminal domain remains firmly bound to the thin filament. The effect of the flexible linker could possibly be to decrease the reaction time when calcium is released into the muscle cell, resulting in faster contraction. Another effect is to allow the two domains to adopt any orientation with respect to one another. Indeed, several cross-linking studies have indicated that when the inhibitory component is bound to TnC, cross-links may be made to helix C of the N-terminal domain (Leszyk et al., 1990; Wang et al., 1990; Kobayashi et al., 1991) which could not be made if the N- and C-terminal domains were fixed as suggested by the X-ray crystallographic structures. One model of the TnC/TnI complex suggests that TnC is elongated (Olah & Trewhella, 1994). Our results neither prove nor disprove this model. From all the results presented thus far on the interaction of these two proteins, it is clear that some sort of flexibility must be present in the central helix to allow the two domains to reorient with respect to one another so that TnC may optimally interact with TnI.

The results presented here suggest that there may be a general mechanism for the activation of proteins which are members of the troponin C family. This group of proteins includes calmodulin and TnC, proteins which need calcium in order to interact with their target proteins in contrast to proteins which are merely calcium buffers such as parvalbumin or calbindin. The first requirement of these proteins is that, in the absence of calcium, the hydrophobic patch is not solvent accessible. Second, upon calcium binding, a large hydrophobic patch which is accessible to solvent should

form to allow the protein to interact with its target. Third, the interhelical connector has to be flexible enough to allow the two domains to adopt any orientation with respect to one another which would allow both domains to interact with their targets in an optimal manner.

Calmodulin and TnC are different in two respects, which is most likely related to the function of these two proteins. First, TnC contains an N-terminal α-helical arm which has been proposed to moderate the destabilization of the central helix, making it less flexible than in calmodulin (Ding et al., 1994). Indeed, if TnC should adopt an elongated conformation in complex with other proteins of the thin filament, a more flexible linker could make complexation more difficult. Second, the C-terminal domain of TnC appears to be different from that of calmodulin. In the absence of calcium, the C-terminal domain of calmodulin remains structured (Finn et al., 1993); however, the C-terminal domain of TnC is not structured. The C-terminal domain of TnC can bind magnesium, and thus when calcium is removed from the muscle cell upon relaxation, the C-terminal domain remains in a similar conformation as when calcium is bound. This would be important in the muscle cell so that TnC would remain firmly anchored to the thin filament during relaxation or contraction. Calmodulin, on the other hand, is not normally permanently bound to any other protein, and thus removal of calcium from the C-terminal sites would ensure that, in the absence of calcium, calmodulin does not interact with its targets.

ACKNOWLEDGMENT

The authors gratefully acknowledge Mr. Stéphane Gagné for many helpful discussions. The authors also thank Dr. Dan Garrett and Dr. Frank Delaglio (NIH) for supplying the programs PIPP and NMRPipe for analyzing and processing the 3D NMR spectra.

SUPPORTING INFORMATION AVAILABLE

One table of ^{1}H, ^{13}C, and ^{15}N side-chain chemical shifts for cloned chicken skeletal troponin C (3 pages). Ordering information is given on any current masthead page.

REFERENCES

Babu, Y. S., Bugg, C. E., & Cook, W. J. (1988) *J. Mol. Biol. 204*, 191.

Babu, A., Rao, V. G., Su, H., & Gulati, J. (1993) *J. Biol. Chem. 268*, 19232.

Barbato, G., Ikura, M., Kay, L. E., Pastor, R. W., & Bax, A. (1992) *Biochemistry 31*, 5269.

Basus, V. J. (1989) *Methods Enzymol. 177*, 132.

Brooks, B. R., Bruccoleri, R. E., Olafson, B. P., States, D. J., Swaminathan, S., & Karplus, M. (1983) *J. Comput. Chem. 4*, 187.

Brünger, A. T. (1992) *X-PLOR 3.1 Manual*, Yale University Press, New Haven, CT.

Carson, M. (1987) *J. Mol. Graphics 5*, 103.

Chandra, M., daSilva, E. F., Sorenson, M. M., Ferro, J. A., Pearlstone, J. R., Nash, B. E., Borgford, T., Kay, C. M., & Smillie, L. B. (1994) *J. Biol. Chem. 269*, 14988.

Chattopadhyaya, R., Meador, W. E., Means, A. R., & Quiocho, F. A. (1992) *J. Mol. Biol. 228*, 1177.

Ding, X., Babu, A., Su, H., & Gulati, J. (1994) *Protein Sci. 3*, 2089.

Dobrowolski, Z., Xu, G., Chen, W., & Hitchcock-DeGregori, S. E. (1991) *Biochemistry 30*, 7089.

Evans, J. S., Levine, B. A., Leavis, P. C., Gergely, J., Grabarek, Z., & Drabikowski, W. (1980) *Biochim. Biophys. Acta 623*, 10.

Finn, B. E., Drakenberg, T., & Forsén, S. (1993) *FEBS Lett. 336*, 368.

Fuchs, F., Liou, Y. M., & Grabarek, Z. (1989) *J. Biol. Chem. 264*, 20344.

Fujimori, K., Sorenson, M., Herzberg, O., Moult, J., & Reinach, F. C. (1990) *Nature 245*, 182.

Gagné, S. M., Tsuda, S., Li, M., Chandra, M., Smillie, L. B., & Sykes, B. D. (1994) *Protein Sci. 3*, 1961.

Gagné, S. M., Tsuda, S., Li, M., Smillie, L. B., & Sykes, B. D. (1995) *Nature Struct. Biol. 2*, 784.

Garrett, D. S., Powers, R., Gronenborn, A. M., & Clore, G. M. (1991) *J. Magn. Reson. 95*, 214.

Gellman, S. H. (1991) *Biochemistry 30*, 6633.

Grabarek, Z., Tan, R. Y., Wang, J., Tao, T., & Gergely, J. (1990) *Nature 345*, 132.

Grabarek, Z., Tao, T., & Gergely, J. (1992) *J. Muscle Res. Cell. Motil. 13*, 383.

Gulati, J., Persechini, A., & Babu, A. (1990) *FEBS Lett. 263*, 340.

Gulati, J., Babu, A., Su, H., & Zhang, Y. (1993) *J. Biol. Chem. 268*, 11685.

Gusev, N. B., Grabarek, Z., & Gergely, J. (1991) *J. Biol. Chem. 266*, 16622.

Heidorn, D. B., & Trewhella, J. (1988) *Biochemistry 27*, 909.

Herzberg, O., & James, M. N. G. (1985) *Biochemistry 24*, 5298.

Herzberg, O., & James, M. N. G. (1988) *J. Mol. Biol. 203*, 751.

Herzberg, O., Moult, J., & James, M. N. G. (1986) *J. Biol. Chem. 261*, 2638.

Hincke, M. T., Sykes, B. D., & Kay, C. M. (1981) *Biochemistry 20*, 3286.

Hubbard, S. R., Hodgson, K. O., & Doniach, S. (1988) *J. Biol. Chem. 263*, 4151.

Hyberts, S. G., Goldberg, M. S., Havel, T. F., & Wagner, G. (1992) *Protein Sci. 1*, 736.

Ikura, M., Kay, L. E., Tschudin, R., & Bax, A. (1990) *J. Magn. Reson. 86*, 204.

Ikura, M., Spera, S., Barbato, G., Kay, L. E., Krinks, M., & Bax, A. (1991) *Biochemistry 30*, 9216.

Ingraham, R. H., & Hodges, R. S. (1988) *Biochemistry 27*, 5891.

Jeener, J., Meier, B. H., Bachmann, P., & Ernst, R. R. (1979) *J. Chem. Phys. 71*, 4546.

Kay, L. E., Marion, D., & Bax, A. (1989) *J. Magn. Reson. 84*, 72.

Kay, L. E., Clore, G. M., Bax, A., & Gronenborn, A. M. (1990) *Science 249*, 411.

Kobayashi, T., Tao, T., Grabarek, Z., Gergely, J., & Collins, J. H. (1991) *J. Biol. Chem. 266*, 13746.

Kraulis, P. J. (1991) *J. Appl. Crystallogr. 24*, 946.

Krudy, G. A., Brito, R. M. M., Putkey, J. A., & Rosevear, P. R. (1992) *Biochemistry 31*, 1595.

Kuszewski, J., Nilges, M., & Brünger, A. T. (1992) *J. Biomol. NMR 2*, 33.

Leszyk, J., Grabarek, Z., Gergely, J., & Collins, J. H. (1990) *Biochemistry 29*, 299.

Levine, B. A., Mercola, D., Coffman, D., & Thornton, J. M. (1977) *J. Mol. Biol. 115*, 743.

Levine, B. A., Thornton, J. M., Fernandes, R., Kelly, C. M., & Mercola, D. (1978) *Biochim. Biophys. Acta 535*, 11.

Li, M. X., Chandra, M., Pearlstone, J. R., Racher, K. I., Trigo-Gonzalez, G., Borgford, T., Kay, C. M., & Smillie, L. B. (1994) *Biochemistry 33*, 917.

Li, M. X., Gagné, S. M., Tsuda, S., Kay, C. M., Smillie, L. B., & Sykes, B. D. (1995) *Biochemistry 34*, 8330.

Lin, X., Krudy, G. A., Howarth, J., Brito, R. M. M., Rosevear, P. R., & Putkey, J. A. (1994) *Biochemistry 33*, 14434.

MacLachlan, L. E., Reid, D. G., & Carter, N. (1990) *J. Biol. Chem. 265*, 9754.

Macura, S., & Ernst, R. R. (1980) *Mol. Phys. 41*, 95.

Meadows, R. P., Nettesheim, D. G., Xu, R. X., Olejniczak, E. T., Petros, A. M., Holzman, T. F., Severin, J., Gubbins, E., Smith, H., & Fesik, S. W. (1993) *Biochemistry 32*, 754.

Murray, A. C., & Kay, C. M. (1972) *Biochemistry 11*, 2622.

Nilges, M., Clore, M., & Gronenborn, A. M. (1988a) *FEBS Lett. 239*, 129.

Nilges, M., Clore, M., & Gronenborn, A. M. (1988b) *FEBS Lett. 229*, 317.

Nilges, M., Gronenborn, A. M., Brünger, A. T., & Clore, G. M. (1988c) *Protein Eng. 2*, 27.
Olah, G. A., & Trewhella, J. (1994) *Biochemistry 33*, 12800.
Pearlstone, J. R., Borgford, T., Chandra, M., Oikawa, K., Kay, C. M., Herzberg, O., Moult, J., Herklotz, A., Reinach, F. C., & Smillie, L. B. (1992a) *Biochemistry 31*, 6545.
Pearlstone, J. R., McCubbin, W. D., Kay, C. M., Sykes, B. D., & Smillie, L. B. (1992b) *Biochemistry 31*, 9703.
Potter, J. D., & Gergely, J. (1975) *J. Biol. Chem. 250*, 4628.
Putkey, J. A., Dotson, D. G., & Mouawad, P. (1993) *J. Biol. Chem. 268*, 6827.
Rance, M., Sørensen, O. W., Bodenhausen, G., Wagner, G., Ernst, R. R., & Wüthrich, K. (1983) *Biochem. Biophys. Res. Commun. 117*, 479.
Reinach, F. C., & Karlsson, R. (1988) *J. Biol. Chem. 263*, 2371.
Satyshur, K. A., Rao, S. T., Pyzalska, D., Drendel, W., Greaser, M., & Sundaralingam, M. (1988) *J. Biol. Chem. 263*, 1628.
Satyshur, K. A., Pyzalska, D., Greaser, M., Rao, S. T., & Sundaralingam, M. (1994) *Acta Crystallogr. D50*, 40.
Slupsky, C. M., Kay, C. M., Reinach, F. C., Smillie, L. B., & Sykes, B. D. (1995a) *Biochemistry 34,* 7365.
Slupsky, C. M., Reinach, F. C., Smillie, L. B., & Sykes, B. D. (1995b) *Protein Sci. 4,* 1279.
Strang, P. F., & Potter, J. D. (1992) *J. Muscle Res. Cell. Motil. 13*, 308.
Sykes, B. D., Slupsky, C. M., Wishart, D. S., Sönnichsen, F. D., & Gagné, S. M. (1995) *NMR as a Structural Tool for Macromolecules: current status and future directions*, Plenum Press, New York (in press).
Vogel, H. J., Lindahl, L., & Thulin, E. (1983) *FEBS Lett. 157*, 241.
Wang, C., Liao, R., & Cheung, H. C. (1993) *J. Biol. Chem. 268*, 14671.
Wang, C. L. A., Zhan, Q., Tao, T., & Gergely, J. (1987) *J. Biol. Chem. 265*, 4953.
Wang, Z., Sarkar, S., Gergely, J., & Tao, T. (1990) *J. Biol. Chem. 265*, 4953.
Wüthrich, K., Billeter, M., & Braun, W. (1983) *J. Mol. Biol. 169*, 949.

BI951586I